Orthogonal Frequency Division Multiplexing Directional Modulation Waveform Design for Integrated Sensing and Communication Systems

Gaojian Huang, *Member, IEEE*, Kailuo Zhang, Yanliang Zhang, Kefei Liao, *Member, IEEE*, Shuanggen Jin, *Senior Member, IEEE*, and Yuan Ding

***Abstract*—Orthogonal frequency division multiplexing (OFDM) signals have been widely studied as a potential waveform used in integrated sensing and communication (ISAC) systems. High-computational effort, however, is required to estimate the azimuth of the target and suppress the interference from the nontarget directions. Moreover, along the nontarget directions, the transmitted confidential information can be easily intercepted by the eavesdroppers. In this article, directional modulation (DM) technology combined with OFDM waveforms, namely, OFDM-DM, is proposed for ISAC systems. From the sensing perspective, the interference from the nontarget direction can be suppressed, and 3-D radar images can be calculated without consuming extra computational resources. From a communication perspective, the OFDM-DM signals provide a secured physical-layer wireless transmission link and thus the confidential information can be securely delivered to the target. The efficacy of the proposed OFDM-DM ISAC waveforms is validated via numerical results for both sensing and communication functionalities by comparison with the traditional OFDM ISAC waveforms.**

***Index Terms*—Directional modulation (DM), integrated sensing and communication (ISAC), orthogonal frequency division multiplexing (OFDM), radar sensing.**

Manuscript received 8 December 2023; revised 20 January 2024; accepted 7 February 2024. Date of publication 19 February 2024; date of current version 6 September 2024. The work of Gaojian Huang was supported in part by the Fundamental Research Funds for the Universities of Henan Province under Grant NSFRF230421, and in part by the Key Scientific Research Projects of Higher Education Institutions in Henan Province under Grant 24A510004. The work of Kefei Liao was supported in part by the Guangxi Science and Technology Department Project under Grant GuikeAB23026120, and in part by the Key Laboratory of Cognitive Radio and Information Processing, Ministry of Education (Guilin University of Electronic Technology) and Guangxi Bagui Scholar Foundation under Grant 2019A51. The work of Shuanggen Jin was supported by the Henan International Science and Technology Cooperation Key Project. The work of Yuan Ding was supported by EPSRC (U.K.) under Grant EP/V002635/1. *(Corresponding author: Shuanggen Jin.)*

Gaojian Huang, Kailuo Zhang, and Yanliang Zhang are with the School of Physics and Electronic Information Engineering, Henan Polytechnic University, Jiaozuo 454003, China (e-mail: g.huang@hpu.edu.cn; 212111010009@home.hpu.edu.cn; ylzhang@hpu.edu.cn).

Kefei Liao is with the School of Information and Communications, Guilin University of Electronic Technology, Guilin 541004, China (e-mail: kefeiliao@guet.edu.cn).

Shuanggen Jin is with the School of Surveying and Land Information Engineering, Henan Polytechnic University, Jiaozuo 454003, China, and also with the Shanghai Astronomical Observatory, Chinese Academy of Sciences, Shanghai 200030, China (e-mail: sgjin@hpu.edu.cn).

Yuan Ding is with the Institute of Sensors, Signals and Systems, Heriot-Watt University, EH14 4AS Edinburgh, U.K. (e-mail: yuan.ding@hw.ac.uk).

Digital Object Identifier 10.1109/JIOT.2024.3367490

I. Introduction

INTEGRATED sensing and communication (ISAC) refers to achieving both wireless sensing and wireless communications functionalities with a single waveform on a transceiver platform. This is possible because the front-end architecture for wireless communications and that for radar sensing systems are becoming more similar [1]. Noted that the ISAC has also been labeled as radar-communications (RadCom) [2], dual-function radar communications [3], or joint radar and communications (JRCs) [4]. Some advantages have been demonstrated in an ISAC system. For example, a communication transmitter can use radar sensing function to locate and/or track the legitimate users for accurate beamforming and/or authentication purpose, thus enhancing the communication performance [5], [6]. On the other hand, with the functionality of wireless communications, the cooperative radar sensor networks can be constructed. The two functionalities of radar sensing and communication therefore benefit each other. They can also share frequency spectrum resources. Thus, the spectral efficiency can be significantly improved [7], [8], [9], [10]. In addition, the ISAC systems could enjoy smaller size and low-cost hardware components due to the high integration [7], [11], [12]. In recent years, the research on ISAC has intensely studied. For example, the ISAC's theoretical boundary in [13] and [14], ISAC design for secure transmissions in [15] and [16], and ISAC assisted environment reconstruction in [17]. One of the biggest challenges in ISAC development is the signal waveform design, which requires delivering information bit streams and achieving radar sensing simultaneously. Conventionally, for radar sensing purpose, the waveforms may require superior autocorrelation properties, while for the better wireless communication, broadband waveforms that support high-data rates are preferred. Thus, the ISAC waveform design needs to strike a balance on functionalities of radar sensing and wireless communications [18]. As for ISAC waveform synthesis, the communication-centric design has attracted a lot of interest [4]. Here, the communication-centric design refers to achieving radar sensing as a secondary function in communication systems, for example, orthogonal frequency division multiplexing (OFDM) ISAC systems reported in [18]. This type of ISAC systems has many potential application scenarios particularly in vehicle-to-vehicle (V2V) or vehicle-to-everything (V2X), where the vehicles sense the

surrounding environment and communications among vehicles and/or infrastructures simultaneously. In [19], the concept of V2V communication and ranging system was first proposed, where spread spectrum technique was adopted to synthesize the radiated signals at the transmitter end. Later, Chirp signals were investigated in ISAC systems [20]. However, achieving high-data rate is difficult for these Chirp ISAC signals. This issue was addressed by using multicarrier signals, such as OFDM [21]. The advantages of OFDM ISAC systems include: low-computational complexity in estimating target Doppler information [22] and the capacity of estimating the time delay and Doppler information for multiple radar targets [23], [24]. However, as is well known, the OFDM signals have high-peak-to-average power ratio (PAPR) that significantly reduces transmitter power efficiency. This also exists in the OFDM ISAC systems. Thus, the constant envelope OFDM (CE-OFDM) ISAC signals with a PAPR of 0 dB were developed in [25]. Meanwhile, the index modulation for OFDM (OFDM-IM) waveforms were also proposed [26]. It has been shown that the OFDM-IM signals can achieve higher spectral efficiency than that of OFDM ISAC systems without consuming additional bandwidth. In the above V2V ISAC systems, however, two problems exist, i.e., high-computational effort is required to estimate the azimuth of the target and suppress the interference from the nontarget directions [27], and information leakage occurs due to the omni-directional information waveforms. Thus, it will pose a threat for the road safety.

Directional modulation (DM), different with the communication security technology in conventional wireless systems in [28] and [29], that are capable of projecting digitally encoded information signals into a prespecified spatial direction while simultaneously distorting the constellation formats of the same signals in all other directions [30]. It can provide a physical layer secured wireless communication. In recent years, different approaches were proposed to synthesize the DM waveforms, such as the far-field array pattern separation approach [31], where the radiated array patterns were divided into two parts, i.e., information and interference patterns, the orthogonal vector approach [32], the MIMO-inspired DM approach [33] and so on. It is worth noting that most of the DM works were forced on the synthesis approaches of the DM waveforms. Until recently, DM waveforms have been found useful in locating targets [34]. Because the bit-error-rate (BER) detected at a transceiver in monostatic arrangement could be used as an indicator of the presence of the targets in free space. Later, the DM waveforms were further studied in locating multiple targets and simultaneously delivering data streams to those targets [35]. On the other research front, time-modulated arrays (TMAs) have been intensively studied in recent years in manipulating its radiation patterns because of its additional degree of freedom in designing the array patterns [36]. TMA was first proposed to synthesize ultralow sidelobe level (SLL) array patterns [37]. Later, different algorithms were developed to optimize the TMA array patterns [38], [39], [40], [41]. Recently, the TMA technique was found useful in many applications, such as beamforming [42], direction findings [43], [44], and DM waveform synthesis [45], [46], [47], [48], [49]. In [49], the three-state TMA was developed to synthesize OFDM-DM waveforms, which can secure the OFDM signals in a preselected direction and distort the constellation points of OFDM signals along all other directions.

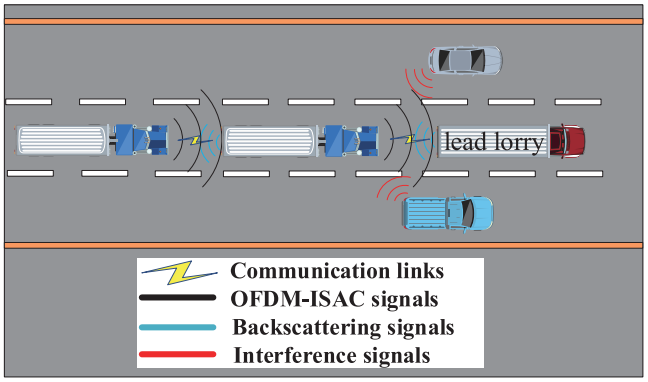

Fig. 1. V2V ISAC application scenario example.

In this article, inspired by the superiorities of DM waveforms in locating targets, we propose the OFDM-DM ISAC scheme. Compared with the popular OFDM ISAC, the advantages can be summarized as follows.

1) The proposed OFDM-DM ISAC waveform scheme not only can obtain the range and relative velocity information but also able to estimate the azimuth of the target by calculating the BER at the transceiver end instead of using the complex algorithms, such as the multiple signal classification (MUSIC) algorithm.
2) The interference from the nontarget directions can be automatically suppressed without consuming additional computational resources in the process of range-velocity radar sensing.
3) The proposed OFDM-DM ISAC signals can project the bit stream information signals only along the target directions, which enables physical-layer security in V2V wireless communications, enhancing road safety.

The remainder of this article is organized as follows. In Section II, the V2V ISAC application scenario examples are first described, followed by the architecture structure of OFDM-DM transceiver and the radar sensing principles. In Section III, simulation results are presented to demonstrate the effectiveness of the proposed scheme, wherein the BERs at the transceiver end are first simulated, followed by the discussions of carrier frequency offset (CFO) effect and the radar sensing performance with suppressed interference from nontarget directions. Finally, conclusions are given in Section IV.

II. Proposed OFDM-DM ISAC Systems

A. V2V ISAC Application Scenario Examples

In Fig. 1, a V2V ISAC application scenario example is depicted, wherein the lead lorry in the platoons is manually driven and it will communicate with the rest of the convoy wirelessly. While other trailing "self-driving" lorries are required to maintain communication links and sense their surroundings using radar technologies. In this application

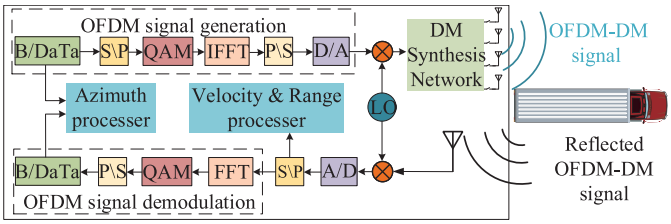

Fig. 2. Architectural block of the proposed OFDM-DM ISAC system.

scenario, the lorries at the back will radiate ISAC signals and receive backscattering signals. From the perspective of communication, the information bit streams mapped onto the ISAC signals need to be securely transmitted to the target lorry. From radar sensing perspective, the target parameters, such as range, relative velocity, and azimuthal angle, need to be estimated from the received backscattering signals. Here, the interference signals from the nontarget directions will be added in the received backscattering signals, seen in Fig. 1.

B. OFDM-DM ISAC System Architecture

In this section, the architectural block of the OFDM-DM ISAC system is introduced, seen in Fig. 2. In the proposed OFDM-DM ISAC system, the transmitter and the receiver are co-located, i.e., monostatic arrangement. The OFDM signals $s(t)$ synthesized at the transmitter end go through the DM synthesis network and radiated by an N-element array, where $s(t)$ can be expressed as

$$s(t) = \sum_{\mu=0}^{N_{\text{sym}}-1} \sum_{n=0}^{N_c-1} a(\mu N_c + n) e^{j2\pi(f_0+f_n)t} \cdot \text{rect}\left(\frac{t-\mu T_{\text{OFDM}}}{T_{\text{OFDM}}}\right) \quad (1)$$

with N_{sym} denoting the total number of transmitted symbols, N_c being the total number of subcarriers in each OFDM symbol, T_{OFDM} being the duration of each total OFDM frame, including a symbol duration T_p and a guard interval duration, $a(\mu N_c + n)$ being a complex number which represents the magnitude and phase states of quadrature amplitude modulation (QAM) scheme of nth subcarrier in the μth OFDM symbol, and $\text{rect}(t/T_{\text{OFDM}})$ describing a rectangular window of duration T_{OFDM}. f_0 denotes the radio frequency (RF) carrier frequency, and f_n is chosen as

$$f_n = nf_p = n/Tp \; n = 0, \ldots, N_c - 1 \quad (2)$$

in order to guarantee the orthogonality.

The OFDM signals pass through the DM synthesis network and its architecture is depicted in Fig. 3. In the proposed DM synthesis network TMA technique is adopted, where the RF switches can be configured as one of three possible states, namely, ON, OFF, and flipping, responding to "+1," "0," and "−1," respectively. $U_k(t)$ is the time domain function of the RF switch that is attached to the kth antenna element. For better illustration, an RF switch function example is shown in Fig. 4. It can be observed that in each RF switch, the parameters σ_k^{on}, $\Delta\sigma_k^{(1)}$, $\Delta\sigma_k^{(2)}$ can be configured. It is assumed that the spacing between each two antenna elements in a linear

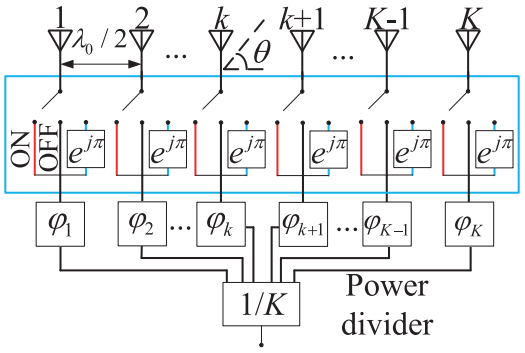

Fig. 3. TMA OFDM-DM transmitter architecture.

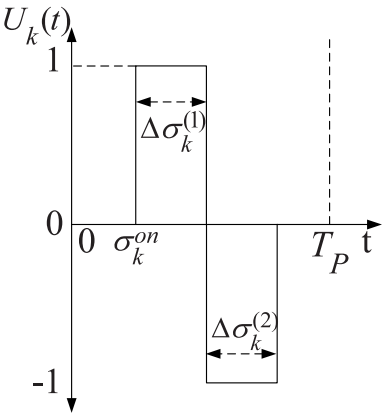

Fig. 4. Illustration of an example RF switch function $U_k(t)$ in time domain.

array is identical and to be $\lambda_0/2$, where λ_0 is the wavelength corresponding to the first OFDM subcarrier frequency f_0. In Fig. 3, φ_k denotes the phase delay in the kth antenna branch, which can be configured to steer the beamforming direction toward where the target is present along θ_{tar}. Here, φ_k is thus designed as in (3)

$$\varphi_k = -(k-1)\pi \cos\theta_{\text{tar}}. \quad (3)$$

The radiated signals from the antenna transmitter end to the far-field can be expressed as

$$E(\theta, t) = \frac{1}{\sqrt{K}} \cdot \sum_{k=1}^{K} \left(s(t) \cdot e^{j\varphi_k} \cdot U_k(t) \cdot e^{j(k-1)\pi\cos\theta} \right). \quad (4)$$

Since $U_k(t)$ is a periodic function, which can be expanded in Fourier series as

$$U_k(t) = \sum_{l=-\infty}^{\infty} c_{lk} e^{j2\pi l f_p t} \quad (5)$$

where c_{lk} is the lth Fourier coefficient for the time sequence function of the kth switch which can be mathematically written as

$$\begin{aligned} c_{lk} &= \frac{1}{T_p} \int_0^{T_p} U_k(t) e^{-j2\pi l f_p t} dt \\ &= \frac{\sin\left(l\pi\Delta\tau_k^{(1)}\right)}{l\pi} e^{-jl\pi\left(2\tau_k^{\text{on}} + \Delta\tau_k^{(1)}\right)} \\ &\quad - \frac{\sin\left(l\pi\Delta\tau_k^{(2)}\right)}{l\pi} e^{-jl\pi\left(2(\tau_k^{\text{on}} + \Delta\tau_k^{(1)}) + \Delta\tau_k^{(2)}\right)}. \end{aligned} \quad (6)$$

In (6), $\tau_k^{\text{on}} = \sigma_k^{\text{on}}/Tp$, $\Delta\tau_k^{(1)} = \Delta\sigma_k^{(1)}/T_p$, and $\Delta\tau_k^{(2)} = \Delta\sigma_k^{(2)}/T_p$, which denote the normalized switch "ON" time instant, the ON time periods of "+1" and "−1," respectively, and $l \in Z$. Substituting (3), (5) and (6) into (4), thus, (4) can be rewritten as

$$E(\theta,t) = \frac{1}{\sqrt{K}} \cdot s(t) \cdot \sum_{l=-\infty}^{\infty} \underbrace{\left[e^{j2\pi l f_p t} \sum_{k=1}^{K} \left(\frac{\sin\left(l\pi\Delta\tau_k^{(1)}\right)}{l\pi} \right.\right.}_{P\left(l,K,\tau_k^{\text{on}},\Delta\tau_k^{(1)},\Delta\tau_k^{(2)},t,\theta\right)} \underbrace{\left.\left. - \frac{\sin\left(l\pi\Delta\tau_k^{(2)}\right)}{l\pi} e^{-jl\pi\left(\Delta\tau_k^{(1)}+\Delta\tau_k^{(2)}\right)} \right)\right.}_{} \underbrace{\left. \cdot e^{-jl\pi\left(2\tau_k^{\text{on}}+\Delta\tau_k^{(1)}\right)} \cdot e^{j(k-1)\pi(\cos\theta-\cos\theta_{\text{tar}})} \right]}_{}. \quad (7)$$

By carefully design these parameters, for example, when (8) is satisfied, the DM symbols can be synthesized along the desired direction θ_{tar}

$$\begin{cases} P\left(l \neq 0, K, \tau_k^{\text{on}}, \Delta\tau^{(1)}, \Delta\tau^{(2)}, t, \theta = \theta_{\text{tar}}\right) = 0 \\ P\left(l = 0, K, \tau_k^{\text{on}}, \Delta\tau^{(1)}, \Delta\tau^{(2)}, t, \theta = \theta_{\text{tar}}\right) \neq 0 \end{cases}. \quad (8)$$

For (8), one of the solution sets is shown in (9) as

$$\begin{cases} \Delta\tau_k^{(1)} \neq \Delta\tau_k^{(2)} \\ \tau_k^{\text{on}},\ \Delta\tau_k^{(1)},\ \Delta\tau_k^{(2)} \in \left\{ \frac{\eta-1}{K} | \eta = 1, 2, \ldots, K \right\} \\ \tau_p^{\text{on}} \neq \tau_q^{\text{on}}, \Delta\tau_p^{(1)} = \Delta\tau_q^{(1)},\ \Delta\tau_p^{(2)} = \Delta\tau_q^{(2)}, \text{when}\ \ p \neq q. \end{cases} \quad (9)$$

When the $\Delta\tau_k^{(1)}$, $\Delta\tau_k^{(2)}$ are set to be independent of k, denoted as $\Delta\tau^{(1)}$, $\Delta\tau^{(2)}$, substituting (9) into (7), along the target direction, the received OFDM-DM signals become

$$E_R(\theta_{\text{tar}}, t) = \left(\Delta\tau^{(1)} - \Delta\tau^{(2)}\right) \cdot \sqrt{K} \cdot s(t). \quad (10)$$

While along other directions, i.e., $\theta \neq \theta_{\text{tar}}$, the received xth subcarriers in the μth OFDM symbol is

$$E_{Rx}(\theta,t) = \frac{1}{\sqrt{K}} \cdot \sum_{n=0}^{N_c-1} \left[a(\mu N_c + n) e^{j2\pi(f_0+nf_p)t} \cdot P\left(l = x-n, K, \tau_k^{\text{on}}, \Delta\tau^{(1)}, \Delta\tau^{(2)}, t, \theta\right) \right]. \quad (11)$$

It can be observed that the data modulated onto the xth subcarrier is corrupted by the random data delivered by all subcarriers. Thus, the transmitted bit information can only be delivered along the desired target direction. Therefore, the BER main beam demodulated from the backscattering signals at the transceiver end can be used as indictor of the direction of radar target [34]. In the proposed OFDM-DM ISAC scheme, it is assumed that the transmitter and receiver are co-located, and the target direction is first to be estimated. Different with the conventional DM, here the synthesized DM beams will be scanning in the angular domain with the help of changing the phase delay in each antenna branch, i.e., configuring φ_k. The detected BER of backscattering signals will drop to a very low value only when the beam scanning direction aligns with the target direction. In this way the unknown targets can be localized, and when the target equips with a suitable receiver, information can be delivered to the target. Actually, in the proposed OFDM-DM ISAC system, the ISAC performs three procedures: 1) scanning; 2) authentication; and 3) estimation. In other words, φ_k is first configured to scan the DM beams, and at the transceiver the possible directions of radar targets can be obtained by observing low-BER beams in spatial domain. To identify the target direction, an authentication operation needs to be performed. Once the target direction is identified, a secure communication link will be constructed, and followed by estimating the range-velocity radar profiles of the target.

C. OFDM-DM ISAC Radar Sensing

In this section, the principle of OFDM-DM ISAC signal waveforms for radar sensing by using the 2-D fast Fourier transform (2-D FFT) approach is introduced. Here, the radar sensing refers to estimating the radar profiles of range and relative velocity of the target. In the proposed OFDM-DM ISAC scheme, once the direction of the target location is identified, a secured communication link from the transmitter to the target along the direction θ_{tar} can be established. It is assumed that a target locates in range R_{tar} and with a Doppler shift f_D due to a relative movement, the backscattering signal at the transceiver can be expressed as (after normalizing out channel attenuation)

$$y(t) = \left(\left(\Delta\tau^{(1)} - \Delta\tau^{(2)}\right) \cdot \sqrt{K}\right) \cdot \sum_{\mu=0}^{N_{\text{sym}}-1} e^{j2\pi f_D t} \sum_{n=0}^{N_C-1} \left(a(\mu N_c + n) e^{j2\pi(f_0+f_n)t} \cdot e^{-j2\pi(f_0+f_n)\frac{2R_{\text{tar}}}{c_0}} \right) \text{rect}\left(\frac{\text{t} - \mu\text{T}_{\text{OFDM}} - \frac{2\text{R}_{\text{tar}}}{\text{c}_0}}{\text{T}_{\text{OFDM}}} \right). \quad (12)$$

In order to obtain the radar profiles of the target, here the 2-D FFT operation is adopted [21], wherein element-wise complex division (EWCD) needs to be first performed to remove the transmitted information from the received information symbols. At the transceiver end, along the target's direction, after EWCD is applied, a matrix $(M_{\text{div1}})_{\mu,n}$ in (13) is obtained in which every column corresponds to one OFDM symbol and every row corresponds to one subcarrier

$$(M_{\text{div1}})_{\mu,n} = \left(\Delta\tau^{(1)} - \Delta\tau^{(2)}\right) \cdot \sqrt{K} \cdot \left(\overrightarrow{z_R} \otimes \overrightarrow{z_D}\right). \quad (13)$$

The operator "⊗" in (13) refers to dyadic product, and

$$\overrightarrow{z_R} = \left(0\ e^{-j2\pi f_p \frac{2R_{\text{tar}}}{c_0}} \ \cdots\ e^{-j2\pi(N_c-1)f_p \frac{2R_{\text{tar}}}{c_0}}\right) \quad (14)$$

$$\overrightarrow{z_D} = \left(0\ e^{j2\pi T_{\text{OFDM}} \frac{2V_{\text{tar}}f_0}{c_0}} \ \cdots\ e^{j2\pi(N_{\text{sym}}-1)T_{\text{OFDM}} \frac{2V_{\text{tar}}f_0}{c_0}}\right). \quad (15)$$

It can be found that, along the target's direction, the information of range and Doppler is well preserved and the information symbols can be completely removed from the backscattering signals. When discrete Fourier transform (DFT)

and inverse DFT (IDFT) operations are, respectively, applied onto every row and column of the matrix $(M_{\text{div1}})_{\mu,n}$, the radar profiles of range R_{tar} and relative velocity V_{tar} can be obtained. While, along the nontarget's directions, $\theta \neq \theta_{\text{tar}}$, when EWCD is applied, the resulting matrix can be expressed as (16), shown at the bottom of the page, where

$$m_{\text{div2}} = \left(\frac{1}{\sqrt{K}} \sum_{n=0}^{N_C-1} \left[P\left(l = x-n, K, \tau_k^{\text{on}}, \Delta\tau^{(1)}, \Delta\tau^{(2)}, t, \theta \right) \cdot a(\mu \cdot N_c + n) \right] \right) \Big/ a(\mu \cdot N_c + n) \tag{17}$$

and "$\odot$" refers to a Hadamard product. In the vector $\overrightarrow{z_R}$, the nth element is $e^{-j2\pi(n-1)f_p([2R_{\text{inter}}]/c_0)}$. Similarly, in the vector $\overrightarrow{z_D}$, the μth element is $e^{j2\pi(\mu-1)T_{\text{OFDM}}([2V_{\text{inter}}f_0]/c_0)}$, where R_{inter} and V_{inter}, respectively, denote the range and relative velocity of the interference sources (e.g., cars). From (16) and (17), it can be observed that the information of range and relative velocity is chaotic, i.e., the linear feature between the elements of every row and column in the matrix is distorted. When 2-D FFT approach is applied for radar imagining, the radar profiles of interference sources will thus be suppressed.

III. Simulation Results and Discussion

A. Estimation of Angular Azimuth

In this section, the angular azimuth of the target vehicle estimated by calculating the BERs at the transceiver with OFDM-DM ISAC signals is shown with its performance analyzed. In the simulation example, it is assumed that $N = 16$, $N_c = 1024$, $N_{\text{sym}} = 256$, $T_p = 11$ us, $T_{\text{OFDM}} = 12.375$ us, $\Delta\xi = |\Delta\tau^{(1)} - \Delta\tau^{(2)}| = 4/16$, and the target vehicle locates in front of the transceiver, i.e., $\theta_{\text{tar}} = 90°$. In Fig. 5, the BERs obtained by demodulating the backscattering binary phase shift keying (BPSK) OFDM-DM signals from the vehicle target are simulated at signal-to-noise ratio (SNR) of 23 dB. Here, SNR is measured along the target vehicle backscattering direction of 90°, and the noise power is assumed identical along every backscattering direction in free space. For comparison purpose, the BERs of radiating traditional BPSK OFDM ISAC signals are also depicted in Fig. 5. It can be observed that high-BER SLLs are present in angular domain in the OFDM ISAC scheme. Thus, the angular azimuth of the target vehicle cannot be given by the BER main beams. While in the proposed OFDM-DM ISAC scheme, it can be observed that only along the target vehicle's direction, a BER main beam is shaped, thus being an indicator of the target direction.

Noted that in a conventional antenna array, to achieve low sidelobes, tapering is normally applied, which can reduce the sidelobes at the expense to the main beam beamwidth. This

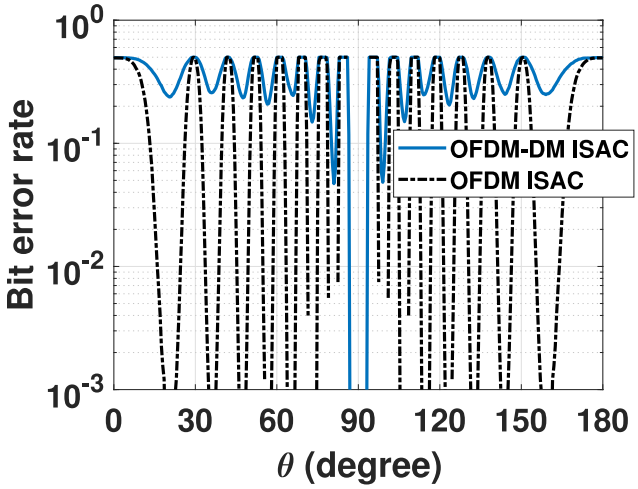

Fig. 5. Calculated BERs of the proposed OFDM-DM and traditional OFDM ISAC schemes at the transceiver end.

may require high-resolution analog-to-digital converter for synthesizing ultralow sidelobes. While, another method to synthesize the desired array patterns, namely, constant modulus shaped beam synthesis approach, can achieve the desired patterns by only changing the phases with a fixed magnitude for each antenna element. Moreover, ultralow sidelobes can also be achieved by using TMA array [37], where "time" is used as a fourth dimension in designing the array patterns through configuring the ON and OFF states of RF switches. In this article, TMA array was employed to synthesize the OFDM-DM symbols. The essence of the OFDM-DM is radiating spatially orthogonal artificial interference that masks/distorts the genuine information. Thus, the low sidelobes indicate that the little artificial interference energy is projected along the sidelobe directions, which would result in widened BER main beam and high-BER sidelobes. Thus, the low-sidelobe patterns are not imperative in synthesizing the TMA OFDM-DM scheme.

In Fig. 6, the BERs of BPSK and QPSK modulated OFDM-DM ISAC schemes are simulated at different SNR levels, where the choices of different SNR levels are equivalent to different distances between the ISAC transmitter vehicle and the target vehicle. It can be observed that at the same SNR level, for example, 15 dB, higher modulation order enjoys narrower BER beamwidth, which indicates better azimuth resolution. Meanwhile, it can be observed that the lower SNR levels the narrower BER beamwidth can be achieved when a same modulation scheme is applied. It is noted that in Fig. 6, the value of $\Delta\xi$ is set to be a constant value of 4/16. In order to study the factors of controlling azimuth resolution, we set different $\Delta\xi$ values in the QPSK OFDM-DM ISAC scheme and the simulation results are depicted in Fig. 7.

$$(M_{\text{div2}})_{\mu,n} = \begin{pmatrix} (m_{\text{div2}})_{\mu=0,n=0} & (m_{\text{div2}})_{\mu=1,n=0} & \cdots & (m_{\text{div2}})_{\mu=N_{\text{sym}}-1,n=0} \\ (m_{\text{div2}})_{\mu=0,n=1} & (m_{\text{div2}})_{\mu=1,n=1} & \cdots & (m_{\text{div2}})_{\mu=N_{\text{sym}}-1,n=1} \\ \vdots & \vdots & \ddots & \vdots \\ (m_{\text{div2}})_{\mu=0,n=N_c-1} & (m_{\text{div2}})_{\mu=1,n=N_c-1} & \cdots & (m_{\text{div2}})_{\mu=N_{\text{sym}}-1,n=N_c-1} \end{pmatrix} \odot \left(\overrightarrow{z_R} \otimes \overrightarrow{z_D} \right). \tag{16}$$

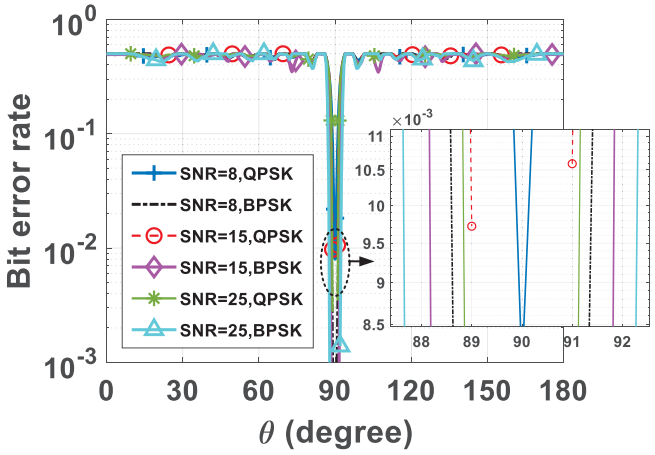

Fig. 6. Calculated BERs of BPSK and QPSK OFDM-DM ISAC schemes with different SNR levels.

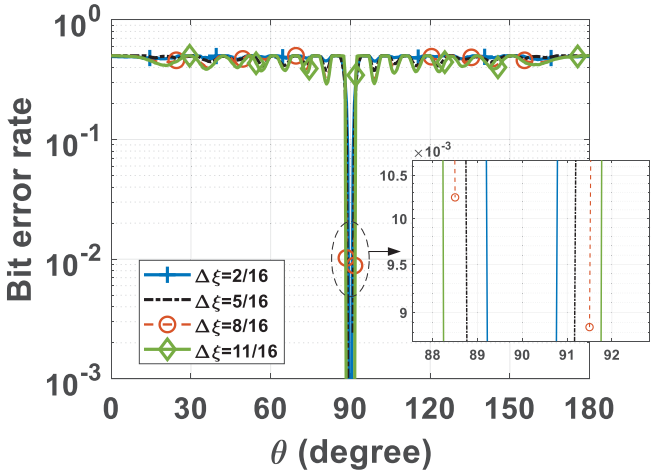

Fig. 7. Calculated BERs of QPSK OFDM-DM ISAC schemes for different $\Delta\xi$ values with SNR = 23 dB.

TABLE I
CALCULATED AZIMUTHAL ANGLE RESOLUTION OF QPSK OFDM-DM SCHEME FOR DIFFERENT $\Delta\xi$ VALUES WITH SNR = 23 dB

$\Delta\xi$ values	Azimuthal angle resolution
2/16	1.1°
5/16	2.0°
8/16	3.0°
11/16	3.2°

In Fig. 7, it can be observed that at a fixed SNR level, the smaller $\Delta\xi$ values correspond to narrower BER beamwidth. In this article, the azimuthal angle resolution is dependent on the DM beamwidth defined as the angle of BER main beam values smaller than 10^{-3}. In the proposed system as shown in Fig. 7, with smaller $\Delta\xi$ values, we have narrower BER beamwidth. In other words, the azimuthal resolution can be flexibly adjusted by setting different $\Delta\xi$ values via controlling the TMA RF switches. For example, when $\Delta\xi = 2/16$, the BER beamwidth is 1.1°, while when $\Delta\xi = 11/16$, the BER beamwidth is 3.2°, see Table I.

From the communication perspective, when the target vehicles are equipped with suitable receivers, information can be delivered to the target vehicle. Because the radiated waveforms are DM signals thus only along the target vehicle direction the correct information is preserved, and along all other directions the constellation diagrams applied onto the OFDM signals are distorted. Thus, it can secure the wireless communication, enabling a high level of road safety.

B. Discussions of Computational Complexity and CFO

In terms of the comparison of computational complexity, in the conventional OFDM ISAC scheme, the azimuthal angle could be obtained by Direction of Arrival (DoA) estimation algorithms. For example, the MUSIC algorithm, which is a subspace-based method that requires the following operations, such as estimating the correlation matrix, finding eigen decomposition of the estimated correlation matrix and the span of noise subspace, and searching larger peaks be performed. These operations will have complexity of $O\{(\beta K^2 + K^3 + (K-\gamma)\cdot K\beta^3)\}$, where β, γ, and K refer to the number of snapshots, signal sources, and antenna elements, respectively. Thus, the MUSIC algorithm has the computational complexity in the order of $O(K^3)$. While in the proposed OFDM-DM ISAC scheme, the BER can be treated as an indicator of the azimuthal angle of the target vehicles. This is because in the OFDM-DM ISAC scheme the transmitter and receiver are assumed to be co-located. When the DM beam direction aligns with the target direction, the detected BER of backscattering signals will drop to a very low value. In this way the azimuthal angle of the target can be estimated, and this approach only needs to calculate the BER values, which is also performed to obtain the received modulation symbol matrix in the OFDM ISAC system. Thus, comparing with the OFDM ISAC scheme, the proposed OFDM-DM ISAC scheme can estimate the target azimuth without consuming additional computational resources. As for radar imaging, the OFDM-DM and OFDM ISAC schemes have similar computational complexity.

From communication perspective, CFO is a problem for the traditional OFDM ISAC communication, which also exists in the OFDM-DM ISAC scheme. Basically, in the OFDM communication system, when the CFO occurs, the received signal will be shifted in frequency, which could result in inter-carrier interference. In Fig. 8, the communication performance of OFDM ISAC systems with CFO is depicted via the metric of error vector magnitude (EVM), whose calculation is chosen to be a standard QPSK constellation pattern. It can be observed that when CFO occurs, it will distort the QPSK constellation patterns, and larger frequency offset will lead to higher levels of distortion. This CFO issue, however, can be estimated and compensated through some approaches, for example, maximum likelihood (ML) estimation. In this approach, the CFO values can be estimated using the long training sequence-preamble, which includes two long symbols, say training symbols # 1 and # 2. The estimated CFO value $\hat{f}_\Delta$ can be given by [50]

$$\hat{f}_\Delta = -\frac{B}{2\pi N_c}\angle\left(\sum_{h=0}^{N_c-1} w_h w_{h+N_c}^*\right) \tag{18}$$

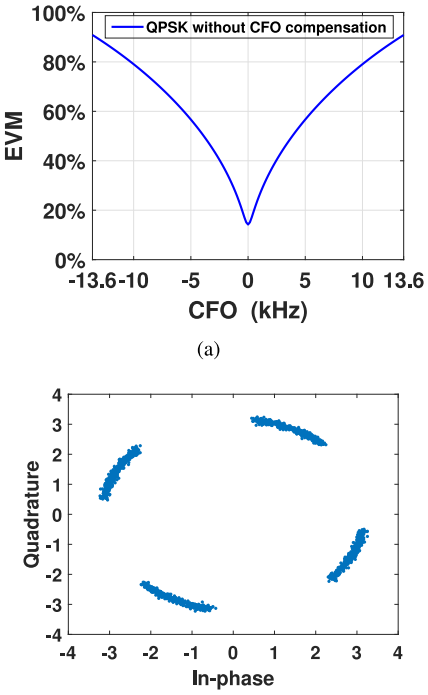

(a) (b)

Fig. 8. CFO for OFDM ISAC (a) EVM versus CFO and (b) distorted QPSK constellation points in in-phase and quadrature (IQ) space.

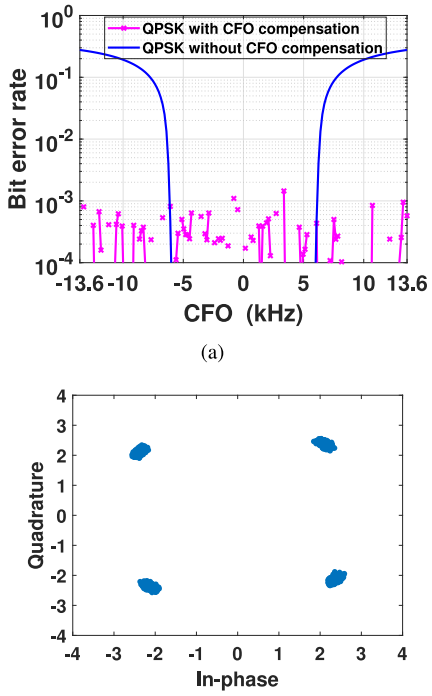

(a) (b)

Fig. 9. Communication performance with CFO compensation (a) BER and (b) QPSK constellation points in IQ space.

where w_h refers to the hth sample point of the received training symbol # 1, which is a complex number, while, w_{h+N_c} denotes the hth sample point of the received training symbol # 2. B is the bandwidth of the OFDM signal, and $B = N_c \cdot f_p$. Notation "$\angle$" denotes the argument of a complex number. It is noted that the range of the estimated CFO by using this ML approach is within $[-B/2N_c, B/2N_c]$, which is [−156.25 kHz, 156.25 kHz] in the 802.11a OFDM standard. Since with a carrier frequency of 24 GHz, the Doppler shift of 1 kHz corresponds to a relative velocity of 6.25 m/s (or, 22.5 km/h). The Doppler shift in V2V applications would be in this range.

When this approach is adopted in the proposed scheme, for example, in Fig. 9, at SNR = 23 dB, the BER along the desired direction is depicted with different CFO values. For comparison purpose, the BER performance without CFO compensation is also depicted. It can be observed that when the CFO is compensated, the BER performance will be significantly improved.

C. Radar Sensing Performance

In this section, the radar profiles of range and relative velocity of the target vehicle are estimated by radiating the OFDM-DM ISAC signals and are compared with those in the OFDM ISAC scheme. Particularly, the anti-interference ability of the OFDM-DM ISAC system is validated. In the simulation examples, the parameters of OFDM are set to be identical with that in Section A. Moreover, it assumed that along the target's direction $R_{\text{tar}} = 45$ m and $V_{\text{tar}} = 25$ m/s, and along the nontarget's directions, we set two interference sources, i.e., two illegitimate cars with the range and relative velocities, respectively, are $R_{\text{inter1}} = 30$ m, $V_{\text{inter1}} = 10$ m/s and $R_{\text{inter2}} = 60$ m, $V_{\text{inter2}} = 35$ m/s. $\Delta\xi$ is set to be a constant value with $\Delta\tau^{(1)} = 15/16$ and $\Delta\tau^{(2)} = 1/16$. In Fig. 10, the radar images in this application example are calculated at SNR level of 23 dB. Here, the SNR is assumed to be 23 dB as an example to keep consistent with that in Section III part A. Since the relative velocity value could be negative, thus, negative relative velocity values also are depicted for

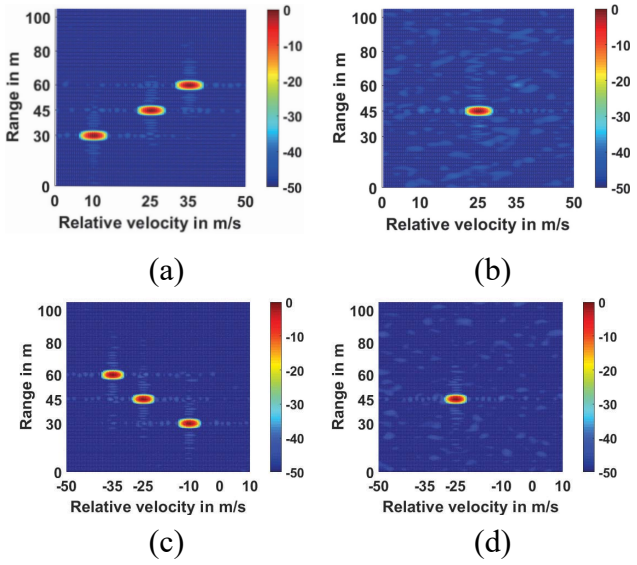

Fig. 10. Radar images obtained by different ISAC schemes at SNR level of 23 dB with $V_{\text{tar}} = 25$ m/s, $V_{\text{inter1}} = 10$ m/s, $V_{\text{inter2}} = 35$ m/s, respectively, for (a) and (b), and $V_{\text{tar}} = -25$ m/s, $V_{\text{inter1}} = -10$ m/s, $V_{\text{inter2}} = -35$ m/s, respectively, for (c) and (d). (a) Traditional OFDM ISAC scheme; (b) proposed OFDM-DM ISAC scheme with $\Delta\tau^{(1)} = 15/16$, $\Delta\tau^{(2)} = 1/16$; (c) traditional OFDM ISAC scheme with negative velocity values; and (d) proposed OFDM-DM ISAC scheme with $\Delta\tau^{(1)} = 15/16$, $\Delta\tau^{(2)} = 1/16$.

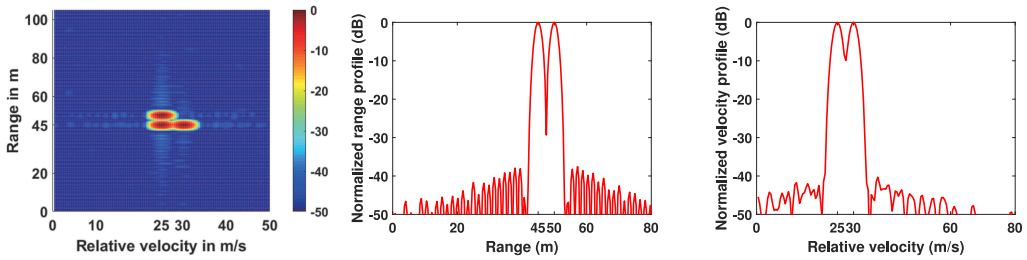

Fig. 11. Radar images obtained by traditional OFDM ISAC scheme at SNR level of 23 dB: (a) range-velocity radar images; (b) 1-D range profiles of the radar images with $V_{\text{inter1}} = 25$ m/s; and (c) 1-D relative velocity profiles of the radar images with $R_{\text{inter2}} = 45$ m.

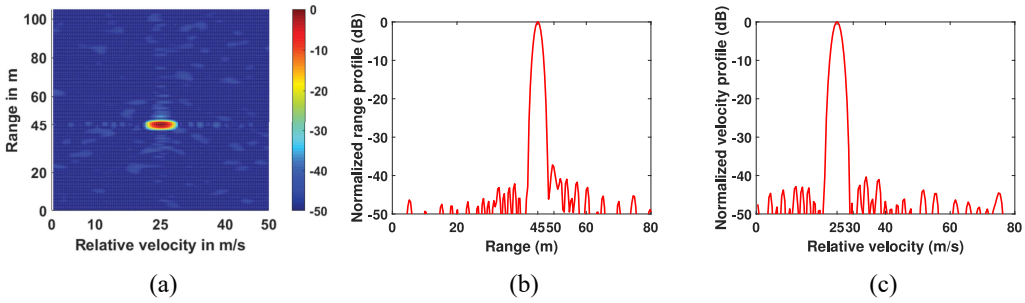

Fig. 12. Radar images obtained by proposed OFDM-DM ISAC scheme at SNR level of 23 dB with $\Delta\tau^{(1)} = 15/16$, $\Delta\tau^{(2)} = 1/16$: (a) range-velocity radar image; (b) 1-D range profile of the radar image with $V_{\text{tar}} = 25$ m/s; and (c) 1-D relative velocity profile of the radar image with $R_{\text{tar}} = 45$ m.

comparison purpose. In Fig. 10(a), it can be observed that by radiating the OFDM ISAC signals three different range-velocity radar images occur, including the target vehicle as well as the two interference sources. Thus, an ambiguity exists in estimating the information of range and relative velocity of the target vehicle in a traditional OFDM ISAC scheme. While, in Fig. 10(b), it can be observed that only the target vehicle's radar image can be calculated, and the ambiguities in range-velocity domain are eliminated in the proposed OFDM-DM ISAC scheme. When the relative velocity is negative value, see in Fig. 10(c) and (d), we have the same conclusion. Thus, whether the relative velocity is positive or negative. The ambiguity problem in a traditional OFDM ISAC scheme can be eliminated in the proposed OFDM-DM ISAC scheme. In other words, the proposed OFDM-DM ISAC scheme can eliminate the target ambiguity issue regardless the Doppler shifter is positive or negative.

For better illustration of the radar sensing performance of the OFDM-DM ISAC system, we set $R_{\text{inter1}} = 50$ m, $V_{\text{inter1}} = 25$ m/s and $R_{\text{inter2}} = 45$ m, $V_{\text{inter2}} = 30$ m/s. In Fig. 11, it can be observed that the ambiguity of the target vehicle still exists in the OFDM ISAC scheme and in Fig. 11(b) and (c), it can be observed that two peaks occurs, which indicate the information of the target vehicle cannot be identified in range and velocity domains. In Fig. 12(b), it can be observed that in the range domain, only a single peak with SLLs of around -40 dB suggests that the target vehicle's range information can be correctly identified and the interference in range domain is suppressed. Similar conclusion can be obtained in the velocity domain, seen in Fig. 12(c). For comparison purpose, the radar images obtained at SNR level of 10 dB is also depicted in Fig. 13. In Fig. 13, it can be observed that SLLs are increased in range and velocity domains at lower SNR levels but the target information of range and relative velocity can still be estimated and identified.

In Fig. 14, the radar images obtained by the OFDM-DM ISAC scheme are depicted with different $\Delta\xi$ values, while other parameter values are kept identical with those in Fig. 12. From Fig. 14, it can be observed that when the value of $\Delta\xi$ increases, the SLLs in range-velocity domain will be suppressed. On the other hand, as we have discussed in Section III-A, a greater $\Delta\xi$ value will lead to a wider BER beamwidth. This is because larger $\Delta\xi$ means higher power efficiency, suggesting that little energy is consumed in the process of radiating orthogonal interference, both in the spatial domain and in the frequency domain. In other words, better radar sensing performance can be obtained with larger $\Delta\xi$ values.

In Fig. 15, the radar range profiles are depicted with $\Delta\xi$ set to be a constant value, say, $\Delta\xi = 5/16$, where $|\Delta\tau^{(1)} - \Delta\tau^{(2)}|$. Here, for the identical $\Delta\xi$, the values of $\Delta\tau^{(1)}$ and $\Delta\tau^{(2)}$ are set to be different for each Figure for comparison purpose. In Fig. 15(d) and (e), it can be observed that lower SLLs could be achieved with smaller values of "$\Delta\tau^{(1)}\Delta\tau^{(2)}$." This is because when "$|\Delta\tau^{(1)} - \Delta\tau^{(2)}|$" is set to be identical, the SLLs of the radar profiles of the target in range and velocity domains are impacted by "$\Delta\tau^{(1)}\Delta\tau^{(2)}$." The larger values of "$\Delta\tau^{(1)}\Delta\tau^{(2)}$," the higher SLLs of the radar profiles will be obtained because the $\Delta\tau^{(1)}\Delta\tau^{(2)}$ determines the power of the injected orthogonal interference.

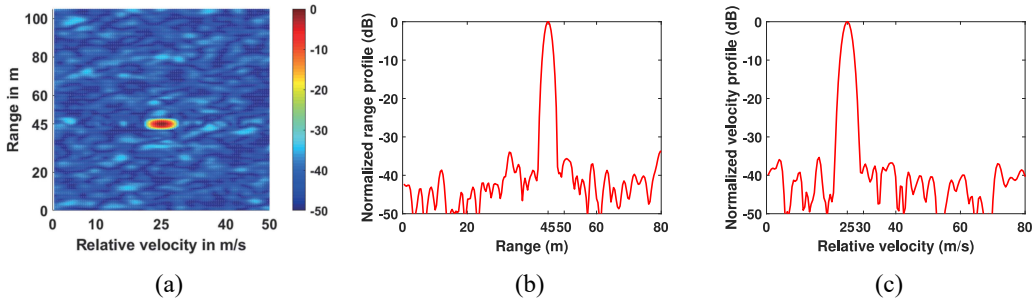

Fig. 13. Radar images obtained by proposed OFDM-DM ISAC scheme at SNR level of 10 dB with $\Delta\tau^{(1)} = 15/16$, $\Delta\tau^{(2)} = 1/16$: (a) range-velocity radar image; (b) 1-D range profile of the radar image with $V_{\text{tar}} = 25$ m/s; and (c) 1-D relative velocity profile of the radar image with $R_{\text{tar}} = 45$ m.

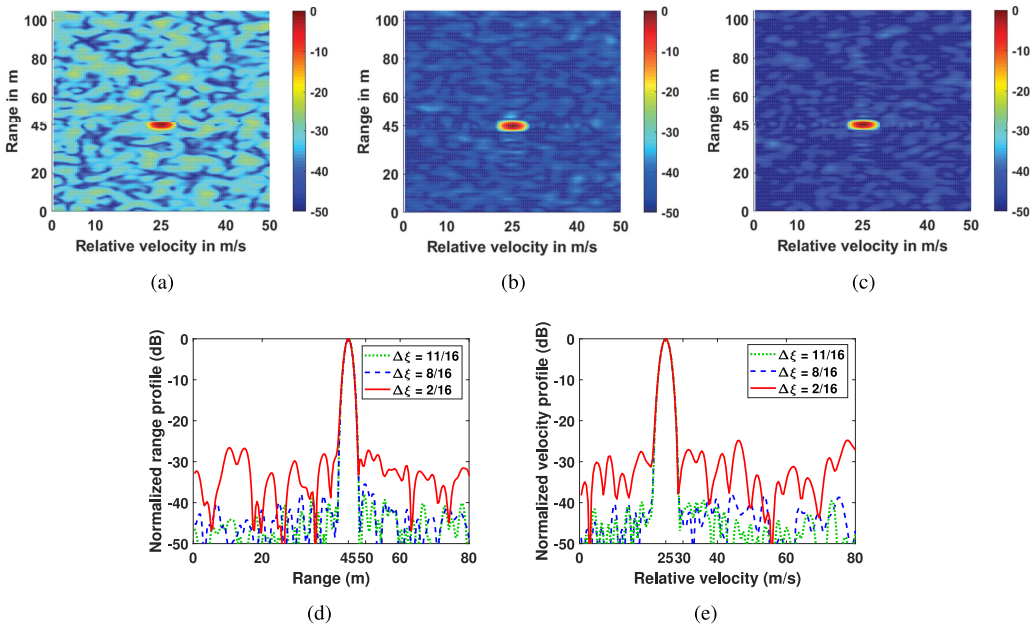

Fig. 14. Radar images obtained by proposed OFDM-DM ISAC scheme at SNR level of 23 dB with (a) $\Delta\xi = 2/16$; (b) $\Delta\xi = 8/16$; (c) $\Delta\xi = 11/16$; (d) 1-D range profile of the radar image with $V_{\text{tar}} = 25$ m/s; and (e) 1-D relative velocity profile of the radar image with $R_{\text{tar}} = 45$ m.

It is noted that in this proposed scheme, we consider a platooning application scenario, which is a typical scenario in practice. In this case, the lorries at the back only need to radiate ISAC signals and sensing the lorries ahead. For each lorry in the platooning, only a single target vehicle needs to be estimated. When we consider a multiple-target scenario, it indicates that the proposed OFDM-DM scheme needs to sensing multiple vehicles. For this purpose, we need to synthesize multiple DM beams simultaneously, and this requires to synthesize multiple nulls with the TMA arrays. For example, for synthesizing two nulls, the optimization algorithms, such as particle swarm optimization, can be used to obtain the solution sets, and configuring the RF switches accordingly. The resulting two DM beams would imping on two target vehicles, and their velocities can be estimated simultaneously. This multiple-target application scenario will be study in the future and will be report in due course.

In the OFDM-DM ISAC systems, from radar sensing perspective, some aspects are now emphasized as follows.

1) The interference signals along the nontarget's directions can be suppressed, and the target ambiguities in range-velocity domain are eliminated.
2) The greater $\Delta\xi$ indicates higher beamforming gains, resulting in lower SLLs of the radar profiles in range and velocity domains.
3) When $\Delta\xi$ is fixed, $\Delta\tau^{(1)}$ and $\Delta\tau^{(2)}$ could be chosen differently. The smaller $\Delta\tau^{(1)}\Delta\tau^{(2)}$ the better radar sensing performance.
4) The values of $\Delta\xi$, $\Delta\tau^{(1)}$ and $\Delta\tau^{(2)}$ could be flexibly controlled in the RF switch functions in the TMAs.

For the ISAC there is a performance tradeoff between the performance of radar sensing and wireless communications. In the proposed scheme, higher beamforming gains could achieve better radar range profiles where the SLLs will be significantly suppressed in range-velocity domain. On the other hand, this would lead to a wider BER beamwidth since less energy is consumed for radiating orthogonal interference. The required tradeoff should be different for various application scenarios. Thus, the flexibility of dynamically changing the tradeoff is

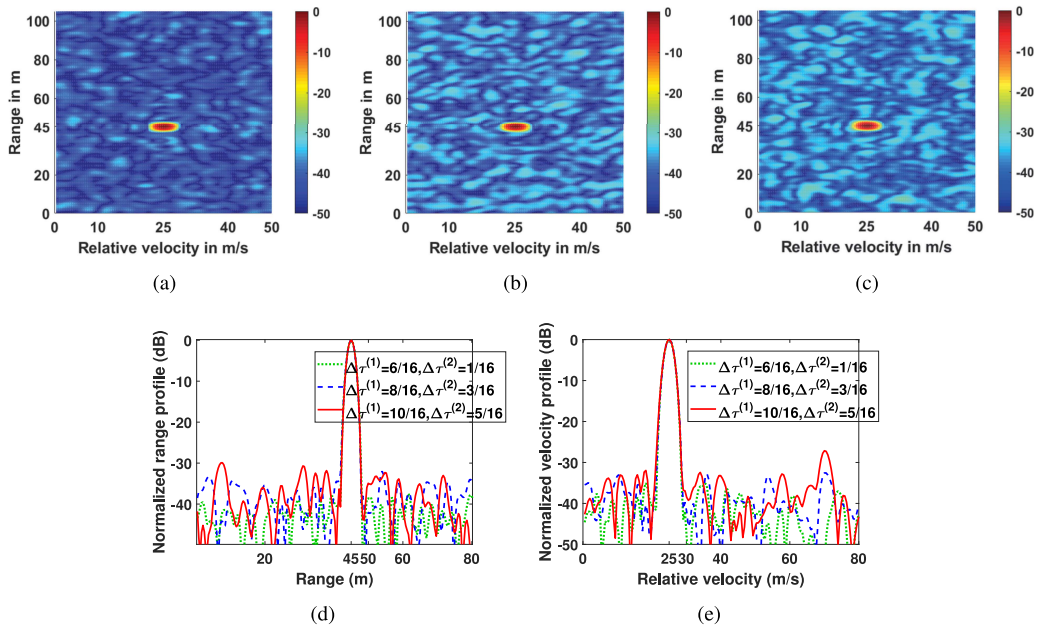

Fig. 15. Radar images obtained by proposed OFDM-DM ISAC scheme at SNR level of 23 dB with (a) $\Delta\tau^{(1)} = 6/16$, $\Delta\tau^{(2)} = 1/16$; (b) $\Delta\tau^{(1)} = 8/16$, $\Delta\tau^{(2)} = 3/16$; (c) $\Delta\tau^{(1)} = 10/16$, $\Delta\tau^{(2)} = 5/16$. (d) 1-D range profile of the radar image with $V_{\text{tar}} = 25$ m/s; and (e) 1-D relative velocity profile of the radar image with $R_{\text{tar}} = 45$ m.

preferable, which, in the proposed scheme, can be achieved by adjusting the values of "$\Delta\tau^{(1)}\Delta\tau^{(2)}$" via RF switches. In this article, we consider a platooning application scenario, in which the two vehicle platoons are required to maintain communication links and sense their surroundings using radar technologies. The channel here is assumed to be Line-of-Sight (LoS), and, the clutter from the nontarget directions would affect the radar performance. This issue can be addressed by the proposed scheme since when we transmit OFDM-DM ISAC signals for radar sensing, the effects of backscattering signals from the nontarget directions would be suppressed. As for the antenna coupling effects, some methods, for example, antenna to antenna isolation and coupling correction, could be used to reduce the coupling effects. In this article, we first propose that OFDM-DM ISAC concept, and show its advantages compared with the OFDM ISAC. We are making efforts to implement proof-of-concept prototypes, and those results will be reported separately in our future work.

IV. Conclusion

In this article, the OFDM-DM waveform signals were proposed for ISAC systems, and the proposed OFDM-DM ISAC scheme here not only inherits the advantages of the popular OFDM ISAC systems but also exhibits promising features, such as 1) using BER as an indicator of the presence of a target; 2) suppressing the interference from the nontarget directions and eliminating the target ambiguity in range and velocity domains; 3) the radar sensing performance can be flexibly adjusted; and 4) finally enabling a level of physical-layer security when communicating to the targets. The proposed OFDM-DM ISAC scheme here therefore is useful in a variety of scenarios, such as V2V, where high-security level and anti-interference ability are required.

References

[1] Y. Cui, F. Liu, X. Jing, and J. Mu, "Integrating sensing and communications for ubiquitous IoT: Applications, trends, and challenges," *IEEE Netw.*, vol. 35, no. 5, pp. 158–167, Sep./Oct. 2021.

[2] J. A. Zhang et al., "An overview of signal processing techniques for joint communication and radar sensing," *IEEE J. Sel. Topics Signal Process.*, vol. 15, no. 6, pp. 1295–1315, Nov. 2021.

[3] A. Hassanien, M. G. Amin, Y. D. Zhang, and F. Ahmad, "Signaling strategies for dual-function radar communications: An overview," *IEEE Aerosp. Electron. Syst. Mag*, vol. 31, no. 10, pp. 36–45, Oct. 2016.

[4] L. G. de Oliveira, B. Nuss, M. B. Alabd, A. Diewald, M. Pauli, and T. Zwick, "Joint radar-communication systems: Modulation schemes and system design," *IEEE Trans. Microw. Theory Techn.*, vol. 70, no. 3, pp. 1521–1551, Mar. 2022.

[5] Z. Xiao and Y. Zeng, "Full-duplex integrated sensing and communication: Waveform design and performance analysis," in *Proc. Int. Conf. Wirel. Commun. Signal Process.*, 2021, pp. 1–5.

[6] Z. Ying, Y. Cui, J. Mu, and X. Jing, "Particle filter based predictive beamforming for integrated vehicle sensing and communication," in *Proc. IEEE Veh Technol Conf.*, 2021, pp. 1–5.

[7] L. Han and K. Wu, "Joint wireless communication and radar sensing systems—State of the art and future prospects," *IET Microw. Antennas Propag.*, vol. 7, no. 11, pp. 876–885, Aug. 2013.

[8] Z. Geng, R. Xu, H. Deng, and B. Himed, "Fusion of radar sensing and wireless communications by embedding communication signals into the radar transmit waveform," *IET Radar Sonar Nav.*, vol. 12, no. 6, pp. 632–640, Jun. 2018.

[9] B. Paul, A. R. Chiriyath, and D. W. Bliss, "Survey of RF communications and sensing convergence research," *IEEE Access*, vol. 5, pp. 252–270, 2017.

[10] X. Wang, A. Hassanien, and M. G. Amin, "Dual-function MIMO radar communications system design via sparse array optimization," *IEEE Trans. Aerosp. Electron. Syst.*, vol. 55, no. 3, pp. 1213–1226, Jun. 2019.

[11] C. W. Rossler, E. Ertin, and R. L. Moses, "A software defined radar system for joint communication and sensing," in *Proc. IEEE Radar Conf.*, 2011, pp. 1050–1055.

[12] M. Labib, V. Marojevic, A. F. Martone, J. H. Reed, and A. I. Zaghloui, "Coexistence between communications and radar systems: A survey," *URSI Radio Sci. Bull.*, vol. 2017, no. 362, pp. 74–82, Sep. 2017.
[13] Z. Zhang, F. Liu, and T. Zhang, "Fundamental limits on integrated sensing and communications frameworks: An IR-UWB case," in *Proc. IEEE Int. Conf. Commun. Workshops (ICC Workshops)*, 2023, pp. 2729–2734.
[14] F. Liu et al., "Integrated sensing and communications: Toward dual-functional wireless networks for 6G and beyond," *IEEE J. Sel Areas Commun.*, vol. 40, no. 6, pp. 1728–1767, Jun. 2022.
[15] Z. Yang, D. Li, N. Zhao, Z. Wu, Y. Li, and D. Niyato, "Secure precoding optimization for NOMA-aided integrated sensing and communication,"*IEEE Trans Commun.*, vol. 70, no. 12, pp. 8370–8382, Dec. 2022.
[16] D. Li, Z. Yang, N. Zhao, Z. Wu, Y. Li, and D. Niyato, "Joint precoding and jamming design for secure transmission in NOMA-ISAC networks," in *Proc. 14th Int. Conf. Wireless Commun. Signal Process. (WCSP)*, 2022, pp. 764–769.
[17] Z. Zhou et al., "6G integrated sensing and communication—Sensing assisted environmental reconstruction and communication," in *Proc. IEEE Int. Conf. Acoust. Speech Signal Process*, 2023, pp. 1–5.
[18] H.-W. Hsu, M.-C. Lee, M.-X. Gu, Y.-C. Lin, and T.-S. Lee, "Analysis and design for pilot power allocation and placement in OFDM based integrated radar and communication in automobile systems," *IEEE Trans. Veh. Technol.*, vol. 71, no. 2, pp. 1519–1535, Feb. 2022.
[19] M. Uchida, Y. Kagawa, and A. Okuno, "A vehicle-to-vehicle communication and ranging system based on spread spectrum technique-SS communication radar," in *Proc. Veh. Navig. Inf. Syst. Conf.*, 1994, pp. 169–174.
[20] M. Roberton and E. Brown, "Integrated radar and communications based on chirped spread-spectrum techniques," in *IEEE MTT-S Int. Microw. Symp. Dig.*, vol. 1, 2003, pp. 611–614.
[21] C. Sturm and W. Wiesbeck, "Waveform design and signal processing aspects for fusion of wireless communications and radar sensing," *Proc. IEEE*, vol. 99, no. 7, pp. 1236–1259, Jul. 2011.
[22] Y. L. Sit, C. Sturm, and T. Zwick, "Doppler estimation in an OFDM joint radar and communication system," in *Proc. Ger. Microw. Conf.*, 2011, pp. 1–4.
[23] D. H. N. Nguyen and R. W. Heath, "Delay and doppler processing for multi-target detection with IEEE 802.11 OFDM signaling," in *Proc. IEEE Int. Conf. Acoust. Speech Signal Process.*, 2017, pp. 3414–3418.
[24] J.-F. Gu, J. Moghaddasi, and K. Wu, "Delay and Doppler shift estimation for OFDM-based radar-radio (RadCom) system," in *Proc. IEEE Int. Wireless Symp.*, 2015, pp. 1–4.
[25] X. Li, L. Tang, and X. Zhang, "Range estimation of CE-OFDM for radar-communication integration," in *Proc. IEEE Int. Conf. Commun. Syst.*, 2018, pp. 131–135.
[26] G. Huang, Y. Ding, S. Ouyang, and V. Fusco, "Index modulation for OFDM RadCom systems," *J. Eng.*, vol. 2021, no. 2, pp. 61–72, Jan. 2021.
[27] Y. L. Sit, B. Nuss, and T. Zwick, "On mutual interference cancellation in a MIMO OFDM multiuser radar-communication network," *IEEE Veh. Technol. Mag.*, vol. 67, no. 4, pp. 3339–3348, Apr. 2018.
[28] X. Li et al., "Hardware impaired ambient backscatter NOMA system: Reliability and security," *IEEE Internet Things J.*, vol. 5, no. 2, pp. 1116–1130, Apr. 2018.
[29] X. Li et al., "Physical-layer authentication for ambient backscatter aided NOMA symbiotic systems," *IEEE Trans. Commun.*, vol. 71, no. 4, pp. 2288–2303, Apr. 2023.
[30] Y. Ding and V. F. Fusco, "A vector approach for the analysis and synthesis of directional modulation transmitters," *IEEE Trans. Antennas Propag.*, vol. 62, no. 1, pp. 361–370, Jan. 2014.
[31] Y. Ding and V. Fusco, "A far-field pattern separation approach for the synthesis of directional modulation transmitter arrays," in *Proc. URSI Gen. Assem. Sci. Symp.*, 2014, pp. 1–4.
[32] Y. Ding and V. Fusco, "Orthogonal vector approach for synthesis of multi-beam directional modulation transmitters," *IEEE Antennas Wireless Propag. Lett.*, vol. 14, pp. 1330–1333, 2015.
[33] Y. Ding and V. F. Fusco, "MIMO-inspired synthesis of directional modulation systems," *IEEE Antennas Wireless Propag. Lett.*, vol. 15, pp. 580–584, 2016.
[34] V. F. Fusco, A. Chepala, and M. A. B. Abbasi, "Target location using dual-beam directional modulated circular array," *IEEE Trans. Antennas Propag.*, vol. 66, no. 12, pp. 7525–7529, Dec. 2018.
[35] G. Huang, Y. Ding, S. Ouyang, and J. M. Purushothama, "Target localization using time-modulated directional modulated transmitters," *IEEE Sensors J.*, vol. 22, no. 13, pp. 13508–13518, Jul. 2022.
[36] S. Yang, Y. B. Gan, and A. Qing, "Sideband suppression in time-modulated linear arrays by the differential evolution algorithm," *IEEE Antennas Wireless Propag. Lett.*, vol. 1, pp. 173–175, 2002.
[37] Q. Chen, J.-D. Zhang, W. Wu, and D.-G. Fang, "Enhanced single-sideband time-modulated phased array with lower sideband level and loss," *IEEE Trans. Antennas Propag.*, vol. 68, no. 1, pp. 275–286, Jan. 2020.
[38] J. Fondevila, J. Bregains, F. J. A. Pena, and E. M. Piquero, "Optimizing uniformly excited linear arrays through time modulation," *IEEE Antennas Wireless Propag. Lett.*, vol. 3, pp. 298–301, 2004.
[39] S. Yang, Y. B. Gan, A. Qing, and P. K. Tan, "Design of a uniform amplitude time modulated linear array with optimized time sequences," *IEEE Trans. Antennas Propag.*, vol. 53, no. 7, pp. 2337–2339, Jul. 2005.
[40] G. Li, S. Yang, Y. Chen, and Z.-P. Nie, "A novel electronic beam steering technique in time modulated antenna array," *Progr. Electromagn. Res.*, vol. 97, pp. 391–405, Oct. 2009.
[41] Y. Gao et al., "Single-sideband time-modulated phased array with 2-bit phased shifters," in *Proc. IEEE Asia-Pac. Conf. Antennas Propag.*, 2020, pp. 1–2.
[42] L. Poli, P. Rocca, G. Oliveri, and A. Massa, "Harmonic beamforming in time-modulated linear arrays," *IEEE Trans. Antennas Propag.*, vol. 59, no. 7, pp. 2538–2545, Jul. 2011.
[43] J. Chen et al., "Direction finding of linear frequency modulation signal in time modulated array with pulse compression," *IEEE Trans. Antennas Propag.*, vol. 68, no. 1, pp. 509–520, Jan. 2020.
[44] C. He, X. Liang, Z. Li, J. Geng, and R. Jin, "Direction finding by time-modulated array with harmonic characteristic analysis," *IEEE Antennas Wireless Propag. Lett.*, vol. 14, pp. 642–645, 2015.
[45] H. Li, Y. Chen, and S. Yang, "Directional modulation in time-modulated array with a novel pseudorandom ascending phase time sequence," *IEEE Trans. Microw. Theory Techn.*, vol. 70, no. 6, pp. 3319–3328, Jun. 2022.
[46] J. Guo, L. Poli, M. A. Hannan, P. Rocca, S. Yang, and A. Massa, "Time-modulated arrays for physical layer secure communications: Optimization-based synthesis and experimental assessment," *IEEE Trans. Antennas Propag.*, vol. 66, no. 12, pp. 6939–6949, Dec. 2018.
[47] H. Li, Y. Chen, and S. Yang, "Chaotic-enabled phase modulation in time-modulated arrays for secure transmission," *IEEE Trans. Antennas Propag.*, vol. 70, no. 11, pp. 10454–10464, Nov. 2022.
[48] Y. Ding, V. Fusco, J. Zhang, and W.-Q. Wang, "Time-modulated OFDM directional modulation transmitters," *IEEE Veh. Technol. Mag.*, vol. 68, no. 8, pp. 8249–8253, Aug. 2019.
[49] G. Huang, Y. Ding, S. Ouyang, and V. Fusco, "Three-state time-modulated array-enabled directional modulation for secure orthogonal frequency-division multiplexing wireless transmission," *IET Commun.*, vol. 16, no. 19, pp. 2321–2327, Sep. 2022.
[50] J. J. van de Beek, M. Sandell, and P. O. Borjesson, "ML estimation of time and frequency offset in OFDM systems," *IEEE Trans. Signal Process.*, vol. 45, no. 7, pp. 1800–1805, Jul. 1997.

Gaojian Huang (Member, IEEE) received the bachelor's degree in electronic information engineering and the Ph.D. degree in information and communications engineering from Guilin University of Electronic Technology, Guilin, China, in 2013 and 2021, respectively.

From October 2017 to October 2018, he was a Visiting Researcher with Queen's University Belfast, Belfast, U.K. He is currently a Lecturer with the School of Physics and Electronic Information Engineering, Henan Poly technic University, Jiaozuo, China. His research interests include integrated sensing and wireless communication designs, antenna array, physical-layer security, emerging modulation techniques, and 5G/6G related areas.

Kailuo Zhang received the B.Sc. degree in communication and information systems from the School of Information Engineering, Beijing Institute of Petrochemical Technology, Beijing, China, in 2019. He is currently pursuing the M.Sc degree in communication and information systems with the School of Physics and Electronic Information Engineering, Henan Polytechnic University, Jiaozuo, China.

His current research interests include directional modulation, and integrated sensing and communication.

Yanliang Zhang received the B.Sc. degree from Henan University, Kaifeng, China, in 2001, and the Ph.D. degree from the School of Electronic Engineering, Xidian University, Xi'an, China, in 2011.

He is currently a Professor with the School of Physics and Electronic Information Engineering, Henan Polytechnic University, Jiaozuo, China. His research interests include machine vision and affective computing.

Kefei Liao (Member, IEEE) received the M.E. and Ph.D. degrees in signal and information processing from the University of Electronic Science and Technology of China, Chengdu, China, in 2010 and 2016, respectively.

He is currently a Master's Supervisor with the School of Information and Communications, Guilin University of Electronic Technology, Guilin, China. His research interests include radar imaging, RCS measurement, and cognitive radar.

Shuanggen Jin (Senior Member, IEEE) was born in Anhui, China, in 1974. He received the B.Sc. degree in geodesy from Wuhan University, Wuhan, China, in 1999, and the Ph.D. degree in geodesy from the University of Chinese Academy of Sciences (CAS), Beijing, China, in 2003.

He is currently a Vice President and a Professor with Henan Polytechnic University, Jiaozuo, China, and also a Professor with Shanghai Astronomical Observatory, CAS, Shanghai, China. He has over 500 articles in peer-reviewed journals and proceedings, ten patents/software copyrights, and ten books/monographs with more than 9000 citations, and H-index >50. His main research areas include satellite navigation, remote sensing, space geodesy, and space/planetary exploration.

Prof. Jin has received One First-Class and Four Second-Class Prizes of Provincial Awards, 100-Talent Program of CAS in 2010, a Fellow of IAG in 2011, Fu Chengyi Youth Science and Technology Award in 2012, the Xia Jianbai Award of Geomatics in 2014, a member of the Russian Academy of Natural Sciences in 2017 and the European Academy of Sciences in 2018, an IUGG Fellow in 2019, a member of Academia Europaea in 2019 and the Turkish Academy of Sciences in 2020, the World Class Professor of Ministry of Education and Cultures, Indonesia in 2021, and a Fellow of Electromagnetics Academy, USA, in 2021. He was a President of the International Association of Planetary Sciences from 2013 to 2017 and the International Association of CPGPS from 2016 to 2017, the Chair of IUGG Union Commission on Planetary Sciences from 2015 to 2023, a Vice President of the IAG Commission 2 from 2015 to 2019, a Vice Chair of COSPAR's Panel on Satellite Dynamics from 2016 to 2020, and the Advances in Space Research from 2013 to 2017, and has been an Editor-in-Chief of the *International Journal of Geosciences* since 2010, an Associate Editor of IEEE TRANSACTIONS ON GEOSCIENCE AND REMOTE SENSING since 2014, the *Journal of Navigation* since 2014, an Editorial Board Member of the *GPS Solutions* since 2016, the *Journal of Geodynamics* since 2014, and the *Planetary and Space Science* since 2014.

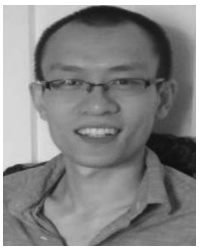

Yuan Ding received the bachelor's degree in electronic engineering from Beihang University, Beijing, China, in 2004, the master's degree in electronic engineering from Tsinghua University, Beijing, in 2007, and the Ph.D. degree in electronic engineering from Queen's University Belfast, Belfast, U.K., in 2014.

He was a Radio Frequency (RF) Engineer with the Motorola Research and Development Centre, Beijing, from 2007 to 2009, before joining Freescale Semiconductor Inc., Beijing, as an RF Field Application Engineer, responsible for high-power base-station amplifier design, from 2009 to 2011. He is currently an Assistant Professor with the Institute of Sensors, Signals and Systems, Heriot-Watt University, Edinburgh, U.K. His research interests are in the IoT-related physical-layer designs, antenna array, physical-layer security, and 5G related areas.

Dr. Ding was the recipient of the IET Best Student Paper Award at LAPC 2013 and the Young Scientists Awards in General Assembly and Scientific Symposium at the 2014 XXXIst URSI.